Indoor Positioning System Using Visible Light and Accelerometer

Muhammad Yasir, *Student Member, IEEE*, Siu-Wai Ho, *Member, IEEE*, and Badri N. Vellambi, *Member, IEEE*

***Abstract*—Indoor positioning system is a critical part in location-based services. Highly precise positioning systems can support different mobile applications in future wireless systems. Positioning systems using existing wireless networks have low deployment costs, but the position error can be up to several meters. While there are positioning systems proposed in the literature that have low position error, they require extra hardware and are therefore costly to deploy. In this paper, we propose an indoor positioning system based on visible light communications (VLC). In contrast to existing works on VLC for positioning, our system estimates the location of the receiver in three dimensions even without: 1) the knowledge of the height of the receiver from ground; and 2) requiring the alignment of the receiver's normal with the LED's normal. Our system has low installation cost as it uses existing lighting sources as transmitters. Light sensor and accelerometer, which can be found in most smartphones, are used at the receiver's side. They are used to measure the received light intensity and the orientation of the smartphone. A low-complexity algorithm is then used to find out the receiver's position. Our system does not require the knowledge of the LED transmitters' physical parameters. Experimental results show that our system achieves average position errors of less than 0.25 m.**

***Index Terms*—Accelerometer, indoor positioning, visible light communications (VLC).**

I. Introduction

THE NEED for a navigation system for both indoor and outdoor settings is increasing day by day. For the outdoor case, Global Positioning System (GPS) is well established, and has been widely used. At different places on the earth, location and time information can be obtained from GPS as long as line-of-sight (LoS) to four or more GPS satellites is available. GPS is very convenient in outdoor settings, but it fails when the signals from GPS satellites are blocked by walls or tall buildings. For example, in urban areas where buildings block the sky view, GPS signal may suffer from deep fading. Further, the GPS error margin can, at times, be of the order of several meters [1], which is not acceptable for indoor settings.

Many alternatives have been proposed for indoor positioning based on visible light, Wi-Fi, infrared (IR), ultrasonic and image sensing [2]–[6]. One of the basic needs in indoor positioning is to provide accurate turn-by-turn navigation to users, which is lacking in existing positioning systems. Some of the existing techniques provide only the proximity area where the user is most likely to be located. Indoor positioning systems based on IR were the first systems to be designed, and are relatively simple [5]. IR-based positioning systems generally use the proximity technique. Some of these systems require many sensors to be installed, making these approaches costly.

Among existing indoor positioning systems, radio frequency (RF) based systems are the most popular; they use existing wireless local area networks to estimate the user coordinates. RF technology provides better coverage than IR- and ultrasonic-based approaches, as RF does not depend on LoS communication. Most RF-based positioning systems are based on fingerprinting or trilateration. The main disadvantage of RF-based fingerprinting is that it is highly environment-dependent, and hence is not robust. For example, the signal strength profile is affected by changes in the background, including the position of objects, addition/removal of objects and access points. Such issues are also associated with IR- and ultrasonic-based positioning systems. Due to multi-path effects and overlapping access points, position error varies between 2 and 5 m [2], which is still significant for indoor settings. In addition, RF-based systems need to be avoided in areas such as hospitals and near airplanes. In [4], a positioning system based on ultrasonic signals is proposed, where time of arrival is used for position estimation. [7] proposes a system that uses RF signals along with ultrasonic signals for synchronization, which makes the approach computationally complex. Another issue is that some positioning systems can track user positions, which raises security and privacy concerns [7].

Visible light communications (VLC), which uses visible light instead of RF electromagnetic waves for communication, has attracted a lot of attention in recent years. Lighting devices are undergoing a revolution transforming from fluorescent lamps or tubes to light emitting diodes (LEDs). Most smartphones and tablets today contain built-in sensors such as photodiodes and accelerometers. In this work, we present a VLC-based positioning system that exploits these technological trends.

This paper is organized as follows. Section II compares our VLC-based positioning system with other VLC-based systems. Section III introduces the system model and the notation used. Section IV explains the proposed algorithm in the two dimensional case. Section IV then explains the working principle and the effect of noise. This is then extended to the three-dimensional algorithm in Section V. Experimental measurement

Manuscript received December 3, 2013; revised June 13, 2014; accepted June 23, 2014. Date of publication July 30, 2014; date of current version August 27, 2014. This paper was presented in part at the 31st Wireless World Research Forum (WWRF 2013) and the 2013 IEEE Global Telecommunications Conference (Globecom 2013).

The authors are with the Institute for Telecommunications Research, University of South Australia, Adelaide, S.A. 5095, Australia (e-mail: muhammad.yasir@mymail.unisa.edu.au; siuwai.ho@unisa.edu.au; badri.vellambi@unisa.edu.au).

Color versions of one or more of the figures in this paper are available online at http://ieeexplore.ieee.org.

Digital Object Identifier 10.1109/JLT.2014.2344772

of accelerometer and photodiode noises and their modelling, simulation and experimental results are presented in Section VI, and the paper is concluded in Section VII.

II. Comparison of the Proposed Positioning System With Other VLC-Based Systems

Accuracy (i.e., position error) is an important performance criterion for indoor positioning systems. However, there are also other performance metrics (see [7] and [8]) to be considered along with accuracy when comparing different positioning systems. Since this work derives a positioning system based on VLC and accelerometer measurements (for estimating receiver's acceleration and orientation), we modify the list of performance metrics in [7], [8] for comparing VLC-based positioning systems. The parameters are as follows:

1) Accuracy.
2) User privacy.
3) Complexity.
4) Cost.
5) Receiver's field of view (FoV) requirement(s).
6) Partial knowledge of the receiver's position.
7) Requirement of the receiver being horizontal.
8) The knowledge of the transmitters' parameters.

The remarkable features of the proposed VLC-based positioning system in the same order as the above list are:

1) The maximum error in the receiver's position estimate is 0.3 m in a space of $5 \times 3 \times 3$ m.
2) Receiver's position is calculated at the receiver side. Hence, the system raises no privacy concern.
3) The positioning system uses a low-complexity algorithm; all calculations have closed-form expressions, and involve only matrix and trigonometric operations.
4) The system is cost-effective, since it uses existing lighting system as transmitters, and sensors commonly found in most smartphones and tablets at the receiver's side.
5) A wide receiver's FoV (1.22 rad) is acceptable in our system.
6) Positioning algorithm does not need the partial knowledge of the receiver's position (e.g., height).
7) Receiver's orientation need not to be horizontal.
8) The system does not require the knowledge of the transmitters' Lambertian parameters and transmit powers.

Some existing VLC-based indoor positioning systems report good positioning accuracy of up to a few centimetres by assuming knowledge of the height of the receiver from the ground [11]–[13]. The same assumption is also used in [12]. Another common assumption in the literature is that the transmitter and receiver axes are both aligned and normal to the ceiling [11], [12]. If the receiver is a mobile phone held by hand, both these assumptions may not be met. Our system, on the other hand, neither requires the knowledge of the receiver's height, nor does it require that the transmitter and the receiver be aligned to the ceiling. However, our positioning system requires that the transmitters are all fixed at almost the same height from the ground. Unlike the approaches in [11], [13], which only estimate the coordinates of the receiver in two dimensions, our positioning scheme estimates the position of the receiver in 3-D, and results show that position error of a few centimeters is achievable when the receiver is under three LEDs and is pointed towards them.

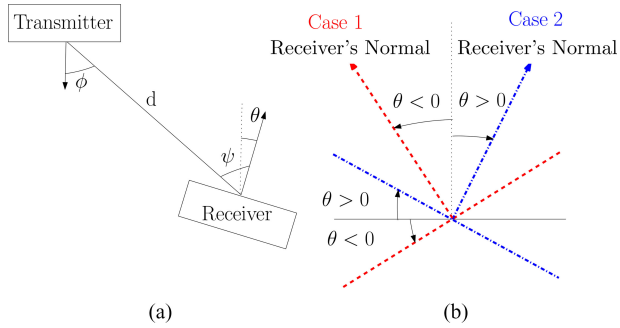

Fig. 1. (a) A transmitter-receiver pair. (b) Orientation angles.

A sensor-assisted indoor positioning system has been proposed in [14]. By considering the maximum receiver FoV of 0.43 rad, the positioning accuracy in the range of 0.3 m to 0.5 m was reported. Note that positioning accuracy decreases with the increase in receiver's FoV. Our positioning algorithm tested with a receiver whose FoV equals 1.22 rad offers an average position error of 0.25 m. Hence, our system allows a larger FoV for the same accuracy when compared with [14].

An indoor positioning system that uses the difference in received optical power due to the difference in angle of arrival is proposed in [15]. Position errors of less than 0.04 m have been reported, however, the work is based on the assumption that receiver's gain profile for each transmitter is known. The receiver's gain profile depends on the environment and the positions of LEDs. Hence, the proposed system is also environment-dependent. Another positioning algorithm based on differential photosensor is presented in [16].

In [17], positioning accuracy of less than 0.01 m has been reported based on simulations alone. The positioning system uses the phase difference of the received signals from multiple transmitters, and is based on LoS communication. In practical settings, signals can be reflected by multiple surfaces/objects and a multi-path model is more appropriate. Since different paths will be affected by different phase delays, the accuracy of the system will be severely reduced in practice.

III. Notation and System Model

The proposed positioning algorithm requires at least two LED light sources fixed at the same height from the ground. However, in our experiments, we use three LED light sources that are in the LoS of the receiver. The LED light sources are the transmitters, and the receiver is a mobile device equipped with a photodiode and an accelerometer. Consider a pair of transmitter and receiver separated by a distance d as shown in Fig. 1(a). Here, ϕ is the *irradiance angle* w.r.t. the transmitter's normal and ψ is the *incidence angle* w.r.t. the receiver's normal. All angles are measured clockwise, and lie in $(-\frac{\pi}{2}, \frac{\pi}{2})$. For example, both ϕ and ψ are negative in Fig. 1(a). Note that the receiver need not be horizontal. Let θ be the *orientation angle*, i.e., the angle

between the receiver's normal and the vertical. Fig. 1(b) shows two examples illustrating the sign of the angles depending on the orientation of the receiver's normal w.r.t. the vertical.

Since LEDs have a large beam divergence, we can model them as Lambertian sources [18]. The channel gain of an LoS optical wireless channel [19], [20] is given by

$$G_{\mathrm{LoS}} = \frac{(m+1)\mathtt{A}}{2\pi d^2}\cos^m(\phi)T(\psi)g(\psi)\cos^M(\psi) \tag{1}$$

where the parameters are as follows. Lambertian parameters m, M are given by $m = \frac{-\log 2}{\log(\cos(\phi_{1/2}))}$ and $M = \frac{-\log 2}{\log(\cos(\psi_{1/2}))}$, where $\phi_{1/2}$ and $\psi_{1/2}$ are the half-power angles of LED and receiver photodiode, respectively. The effective area of the photodiode at the receiver is given by $\mathtt{A}$. The filter gain and concentrator gain are represented by $T(\psi)$ and $g(\psi)$, respectively. When the transmitter's optical flux is Φ_T, (in lumens), the received optical power[1] is $P_{\mathrm{LoS}} = \Phi_T G_{\mathrm{LoS}}$ (in lux $\cdot$ m^2). In this work, we assume that no filter or concentrator is used at the receiver (i.e., $T(\psi) = g(\psi) = 1$). Hence, we may assume without the loss of generality that the optical power P_{LoS} (in lux $\cdot$ m^2) incident on the receiver is

$$P_{\mathrm{LoS}} = \frac{C}{d^2}\cos^m(\phi)\cos^M(\psi) \tag{2}$$

where $C \triangleq \frac{(m+1)\mathtt{A}\Phi_T}{2\pi}$ depends on the physical aspects of the LED and the photodiode, and is independent of the orientation. In optical wireless setups such as the one considered here, it is possible that the total incident optical power P_R (in lux $\cdot$ m^2) is from LoS and non-LoS paths [19], i.e.,

$$P_R = P_{\mathrm{LoS}} + P_{\mathrm{NLoS}} + P_{\mathrm{Background}} \tag{3}$$

where $P_{\mathrm{Background}}$ is the incident optical power due to other light sources in the background, and P_{NLoS} is the incident optical power form the transmitter, but due to non-LoS paths. The details of how to calculate P_{NLoS} is given in [19].

The total incident power can be measured by means of the average electric current μ_{I_R} (in Amperes) generated by the photodiode, since $\mu_{I_R} = \frac{R_p P_R}{\mathtt{A}}$, where R_p is the responsivity of the photodiode. Even though this equation seems to indicate that the average photodiode current is inversely proportional to the effective area $\mathtt{A}$, it should be noted that both R_p and P_R are directly proportional to $\mathtt{A}$. Hence, the average current is directly proportional to $\mathtt{A}$. The photodiode current is affected by two noise processes: 1) *shot noise*, i.e., fluctuations in the current due to incident optical power consisting of the desired signal and ambient light source; and 2) *thermal noise*, i.e., fluctuations in the current due to the random motion of electrons, and changes with the absolute temperature of the electric circuit. The total noise variance $\sigma^2_{\mathrm{noise}}$ (in A^2) in electric current domain is given by

$$\sigma^2_{\mathrm{noise}} = \sigma^2_{\mathrm{thermal}} + \sigma^2_{\mathrm{shot}} \tag{4}$$

where σ^2_{shot} depends on P_{LoS}, P_{NLoS}, $P_{\mathrm{Background}}$, and R_p, and $\sigma^2_{\mathrm{thermal}}$ is independent of the incident power. The effective signal-to-noise ratio (SNR) in the electric current domain due to the LoS component is defined as

$$\mathrm{SNR(dB)} = 10\log_{10}\frac{(R_p\frac{P_{\mathrm{LoS}}}{\mathtt{A}})^2}{\sigma^2_{\mathrm{noise}}}. \tag{5}$$

This work assumes that the LoS path is the main contributor to total optical power incident on the receiver, and calculates the total optical power using (2).

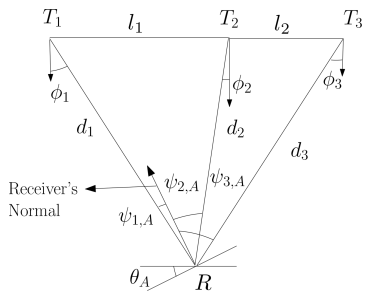

Fig. 2. The orientation of the transmitters and the receiver.

IV. Localization in Two-Dimensional Case

In our system, the received optical power is used to estimate distances between the receiver and the transmitters. We measure the received power from each transmitter twice by varying only the receiver orientation. The measurements are used to identify the irradiance angles at transmitters, which are then used to identify distance using triangulation and trigonometry. Using the distances, the position estimate is then obtained.

Note that the received power given by (2) depends not only on the distance, but also on the irradiance and incidence angles. By fixing the receiver's position, and by changing only the orientation, the received power P_{LoS} changes due to changes in the incident angle ψ. Thus, the orientation of the receiver is also important. The accelerometer in the receiver will be used to determine the receiver's orientation, and eventually, the incidence and irradiance angles.

In our system, Transmitters T_1, T_2 and T_3 are installed in the ceiling of a room as shown in Fig. 2. For the sake of simplicity, this section presents the analysis for the two-dimensional case. The three-dimensional case will be dealt with in Section V. Let for $1 \le i \le 3$, d_i be the distance between Transmitter T_i and the Receiver R. Let ϕ_i be the irradiance angle w.r.t. the normal to the ceiling at Transmitter T_i. We assume that each transmitter knows its coordinates and broadcasts the coordinates to the receiver via VLC. We also assume that the receiver can estimate the received power from each transmitter by approaches such as time division multiple access (TDMA).

Two measurements (Measurements A and B) are made at the receiver at approximately the same position but with different orientations. This can be done by merely rotating the mobile device by a small angle[2]. Let the corresponding orientation

[1]Here, we use the photometric unit lux$\cdot$m^2 for power. Physical units lux $\cdot$ m^2 and Watts are interchangeable and the constant for conversion depends on the device. For the photodiode used in this work, 1 lux $\cdot$ m^2 $= 0.05$ W [22].

[2]Alternatively, multiple photodiodes with different tilt angles can be built into the receiver to take measurements simultaneously; this will equivalently simulate different receiver's normal as illustrated in Fig. 1(b).

angles be denoted by θ_A and θ_B, respectively. For Measurements A and B, let $\psi_{i,A}$ or $\psi_{i,B}$ denote the incident angles (on the LoS path) w.r.t. the corresponding receiver normals, and let the received powers be denoted by $P_{i,A}$ and $P_{i,B}$. Note that $\psi_{i,A}$, θ_A and ϕ_i are related by

$$\psi_{i,A} = \phi_i - \theta_A \tag{6}$$

regardless of whether the transmitter is to the left or the right side of the receiver as shown in Fig. 2. Similarly, we have

$$\psi_{i,B} = \phi_i - \theta_B. \tag{7}$$

Hence

$$\psi_{i,B} = \psi_{i,A} + \theta_A - \theta_B. \tag{8}$$

Note that the receiver uses the photodiode to estimate incident powers $P_{i,A}$ and $P_{i,B}$, and the accelerometer to obtain orientation angles θ_A and θ_B. From these measurements, our approach first estimates ϕ_i, $i = 1, 2, 3$. Together with the coordinates of the transmitters, the receiver can then locate itself. The following theorem illustrates how ϕ_i can be found.

Theorem 1: Suppose that $P_{i,A}, P_{i,B}$ are known exactly for each $i = 1, 2, 3$, and that the orientation angles θ_A and θ_B are also known precisely. Let M be the Lambertian parameter of the receiver. Then, for each $i = 1, 2, 3$,

$$\phi_i = \theta_A + \arctan\left(\frac{P_{i,B}^{\frac{1}{M}} - P_{i,A}^{\frac{1}{M}}\cos(\theta_B - \theta_A)}{P_{i,A}^{\frac{1}{M}}\sin(\theta_B - \theta_A)}\right). \tag{9}$$

Proof: Using (2), we see that the received power from Transmitter T_i, $i = 1, 2, 3$ in Measurements A and B are

$$P_{i,A} = \frac{C}{d_i^2}\cos^m\phi_i\cos^M\psi_{i,A}, \tag{10}$$

$$P_{i,B} = \frac{C}{d_i^2}\cos^m\phi_i\cos^M\psi_{i,B}. \tag{11}$$

Hence

$$P_{i,B}\cos^M\psi_{i,A} = P_{i,A}\cos^M\psi_{i,B} \tag{12}$$

$$\therefore\ P_{i,B}^{\frac{1}{M}}\cos\psi_{i,A} = P_{i,A}^{\frac{1}{M}}\cos\psi_{i,B} \tag{13}$$

$$= P_{i,A}^{\frac{1}{M}}\cos(\psi_{i,A} - (\theta_B - \theta_A)) \tag{14}$$

where in (14), we have used (8). Rearranging terms after using $\cos(\omega_1 - \omega_2) = \cos\omega_1\cos\omega_2 + \sin\omega_1\sin\omega_2$, we get

$$\psi_{i,A} = \arctan\left(\frac{P_{i,B}^{\frac{1}{M}} - P_{i,A}^{\frac{1}{M}}\cos(\theta_B - \theta_A)}{P_{i,A}^{\frac{1}{M}}\sin(\theta_B - \theta_A)}\right). \tag{15}$$

Together with (6), the theorem is proved. ∎

This theorem highlights the following fact: the algorithm does not require the knowledge of the transmit power and Lambertian parameter m of the transmitters. Only the received powers, orientation and Lambertian parameter M of the receiver's photodiode are required. Though the above result is presented for noiseless conditions, we can still use it to estimate incidence and irradiance angles when noise is present.

In the following, we illustrate how to find the distance d_i between the receiver and Transmitter T_i. Using these distances,

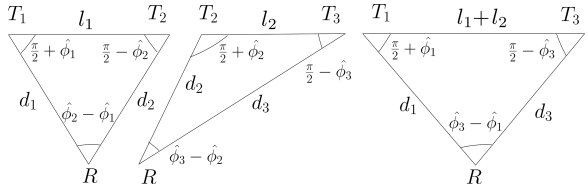

Fig. 3. Sine law can be applied to find d_i. Note that the angle subtended at R can be actually larger than $\frac{\pi}{2}$.

the coordinates of the receiver can then be found. Since the receiver knows the coordinates of the transmitters, the distance between each pair of transmitters is known. Let l_1 be the distance between T_1 and T_2 and let l_2 be the distance between T_2 and T_3. Let for $i = 1, 2, 3$, $\hat{\phi}_i$ be the noisy estimate of the true ϕ_i computed using (9). The error in this estimate is due to both the noise in the communications medium and the devices. From $\hat{\phi}_i$ and l_i, the receiver can construct three triangles $\Delta(T_1T_2R)$, $\Delta(T_2T_3R)$ and $\Delta(T_1T_3R)$ as shown in Fig. 3. From each triangle, we can use the sine law to estimate distances. Let $\hat{d}_1^{(12)}$, $\hat{d}_2^{(23)}$ and $\hat{d}_1^{(13)}$ be the distances obtained from $\Delta(T_1T_2R)$, $\Delta(T_2T_3R)$ and $\Delta(T_1T_3R)$, resp. We have

$$\hat{d}_1^{(12)} = \frac{l_1\cos\hat{\phi}_2}{\sin(\hat{\phi}_2 - \hat{\phi}_1)} \tag{16}$$

$$\hat{d}_2^{(23)} = \frac{l_2\cos\hat{\phi}_3}{\sin(\hat{\phi}_3 - \hat{\phi}_2)} \tag{17}$$

$$\hat{d}_1^{(13)} = \frac{(l_1 + l_2)\cos\hat{\phi}_3}{\sin(\hat{\phi}_3 - \hat{\phi}_1)}. \tag{18}$$

From these distances, the receiver location (x_R, y_R) can be estimated from those of the transmitters using the following.

Definition 1 (Positioning Algorithm for 2-D): Suppose the coordinates of T_1 and T_2 are (x_1, y_1) and (x_2, y_2), respectively. From the estimates $\hat{\phi}_i$, $i = 1, 2, 3$, obtained from (9) and $(\hat{d}_1^{(12)}, \hat{d}_2^{(23)}, \hat{d}_1^{(13)})$ obtained from (16)–(18), define

$$\left(\hat{x}_R^{(12)}, \hat{y}_R^{(12)}\right) = (x_1, y_1) + \hat{d}_1^{(12)}(\cos(\frac{\pi}{2} + \hat{\phi}_1), -\sin(\frac{\pi}{2} + \hat{\phi}_1))$$

$$\left(\hat{x}_R^{(23)}, \hat{y}_R^{(23)}\right) = (x_2, y_2) + \hat{d}_2^{(23)}(\cos(\frac{\pi}{2} + \hat{\phi}_2), -\sin(\frac{\pi}{2} + \hat{\phi}_2))$$

$$\left(\hat{x}_R^{(13)}, \hat{y}_R^{(13)}\right) = (x_1, y_1) + \hat{d}_1^{(13)}(\cos(\frac{\pi}{2} + \hat{\phi}_1), -\sin(\frac{\pi}{2} + \hat{\phi}_1)).$$

The estimated receiver coordinates are given by

$$(\hat{x}_R, \hat{y}_R) = \left(\frac{\hat{x}_R^{(12)} + \hat{x}_R^{(23)} + \hat{x}_R^{(13)}}{3}, \frac{\hat{y}_R^{(12)} + \hat{y}_R^{(23)} + \hat{y}_R^{(13)}}{3}\right).$$

When there is no noise in the system, the estimate $\hat{\phi}_i$ equals the true ϕ_i for each $i = 1, 2, 3$. As a result, the distances estimated also equal the actual distances from the transmitters. Consequently, the position estimates $(\hat{x}_R^{(1)}, \hat{y}_R^{(1)})$, $(\hat{x}_R^{(2)}, \hat{y}_R^{(2)})$, and $(\hat{x}_R^{(3)}, \hat{y}_R^{(3)})$ will be identical. However, due to the noise in the photodiode and accelerometer measurements, instead of these position estimates coinciding as shown in Fig. 4(a), they could be inconsistent as shown in Fig. 4(b). Estimating the receiver

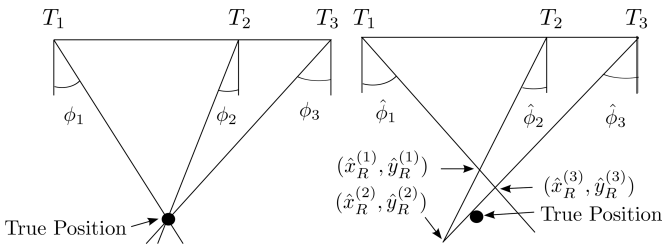

Fig. 4. (a) Ideal case with no noise. (b) Inconsistent solutions due to the error in the estimated $\hat{\phi}_i$.

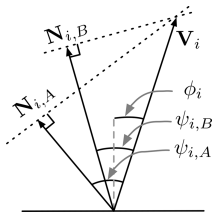

Fig. 5. The method for finding $\mathbf{V}_i$ pointing at Transmitter T_i.

position from these inconsistent solutions is a well-formulated problem in positioning [23], [20]. In Definition 1, we simply use the centroid of the triangle formed by the three estimates as the final estimate of the receiver's position.

V. Positioning Algorithm for 3-D

We start with an alternate but equivalent formulation of the two dimensional positioning given in Section IV. This formulation extends naturally to the three-dimensional case. Consider Fig. 5. Let $\mathbf{U}_i$ be a vector with magnitude $\frac{\Phi_T\,(m+1)A}{2\pi d_i^2}\cos^m(\phi_i)$, pointing towards Transmitter T_i from Receiver R. Let $\mathbf{V}_i$ be a vector of magnitude $|\mathbf{U}_i|^{\frac{1}{M}}$ in the direction of $\mathbf{U}_i$. Let $\mathbf{N}_{i,A}$, $\mathbf{N}_{i,B}$ be the vectors obtained by projecting $\mathbf{V}_i$ onto the receiver's normals in Measurements A and B, resp. Then, for $1 \le i \le 3$,

$$|\mathbf{N}_{i,A}| = |\mathbf{V}_i|\cos\psi_{i,A} = |\mathbf{U}_i|^{\frac{1}{M}}\cos\psi_{i,A} = P_{i,A}^{\frac{1}{M}}. \quad (19)$$

Similarly, $|\mathbf{N}_{i,B}| = \mathbf{P}_{i,B}^{\frac{1}{M}}$. At the receiver, vectors $\mathbf{N}_{i,A}$ and $\mathbf{N}_{i,B}$ can be constructed from the received power and the receiver's orientation (receiver's normal) measured using the accelerometer. Since $\mathbf{N}_{i,A}$ and $\mathbf{N}_{i,B}$ are projections of $\mathbf{V}_i$, by drawing two lines perpendicular to $\mathbf{N}_{i,A}$ and $\mathbf{N}_{i,B}$ that pass through their tips, the vector $\mathbf{V}_i$ can be found. It is interesting to note that we just need to know the ratio of the received powers (or equivalently, $\frac{|\mathbf{N}_{i,A}|}{|\mathbf{N}_{i,B}|}$), and the orientation of the mobile device to determine $\mathbf{V}_i$. This explains why the right-hand side of (9) is fully determined by $\frac{P_{i,A}}{P_{i,B}}$, θ_A and θ_B.

Now, consider the three-dimensional case. Here, we need at least three measurements using three distinct orientations of the receiver. Let $\mathbf{N}_{i,A}$, $\mathbf{N}_{i,B}$ and $\mathbf{N}_{i,C}$ be the vectors obtained by projecting $\mathbf{V}_i$ onto the receiver's normals in Measurements A, B and C, respectively. Let $\Lambda_{i,A}$ be the plane perpendicular to vector $\mathbf{N}_{i,A}$ that passes through the tip (ending point) of $\mathbf{N}_{i,A}$. Planes $\Lambda_{i,B}$ and $\Lambda_{i,C}$ are defined similarly using $\mathbf{N}_{i,B}$ and $\mathbf{N}_{i,C}$. Since the receiver's normals are assumed to be different in the three measurements, the planes $\Lambda_{i,A}$, $\Lambda_{i,B}$ and $\Lambda_{i,C}$ intersect at exactly one point, say ξ_i. Let $\mathbf{V}_i, i = 1, 2, 3$ be the vector starting from the receiver and ending in ξ_i. Since each LED broadcasts its coordinates through VLC, receiver knows the position of all three LEDs. Once all three vectors $\mathbf{V}_i$ are found, we can easily estimate the user's coordinates.

In this case, the ratio of received powers from two distinct measurements $j, k \in \{A, B, C\}$ from Transmitter $T_i, i = 1, 2, 3$ is given by

$$\frac{|\mathbf{N}_{i,j}|}{|\mathbf{N}_{i,k}|} = \frac{|\mathbf{V}_i|\cos\psi_{i,j}}{|\mathbf{V}_i|\cos\psi_{i,k}} = \frac{\cos\psi_{i,j}}{\cos\psi_{i,k}}. \quad (20)$$

Substituting (2) into (20), we get

$$\frac{|\mathbf{N}_{i,j}|}{|\mathbf{N}_{i,k}|} = \left(\frac{P_{i,j}}{P_{i,k}}\right)^{\frac{1}{M}}, \quad i = 1, 2, 3,\ j, k \in \{A, B, C\}. \quad (21)$$

Note that (21) does not require the knowledge of the transmitter LED's Lambertian parameter m. We only need to know the receiver's Lambertian parameter M, received light intensity and the orientation of the receiver. The orientation of the receiver is calculated using accelerometer of the mobile device.

In the three-dimensional case, we need at least three measurements from three different orientations to compute the position of the user. The orientations of the receiver are important for better positioning accuracy, e.g., if the receiver is facing towards the LEDs, the positioning accuracy is higher. However, in practice, due to the noise in the received powers and accelerometer measurements, the planes vary from their actual positions resulting in a noisy estimate of the vector $\mathbf{V}_i$ pointing from the receiver towards the transmitter T_i. In order to minimize the effect of noise, the receiver can record more than three measurements and estimate the position using these measurements. Due to noise, all the planes may not intersect at exactly one point. To define a meaningful estimate, we let $\hat{\mathbf{V}}_{\mathrm{i}}$ to be the vector that is, loosely, the closest to all the planes. Suppose a user rotates the phone in hand and records K different measurements. At the same time, K different orientations are recorded by the accelerometer. Now in this case, we obtain K planes and need to find the vector $\hat{\mathbf{V}}_{\mathrm{i}} = [x_{0,i}\ \ y_{0,i}\ \ z_{0,i}]^T$ using these K planes. Let the K planes for the Transmitter T_i be $L_{i,j} : a_{i,j}X + b_{i,j}Y + c_{i,j}Z = \delta_{i,j},\ j = 1, \ldots, K$. We define the vector $\hat{\mathbf{V}}_{\mathrm{i}} = [\hat{x}_{0,i}\hat{y}_{0,i}\hat{z}_{0,i}]^T$ as the solution to the following minimization problem

$$\hat{\mathbf{V}}_{\mathrm{i}} \triangleq \underset{(x_{0,i}, y_{0,i}, z_{0,i})}{\arg\min} \left(\sum_{j=1}^{K} d_{\min}^2\left[(x_{0,i}, y_{0,i}, z_{0,i}), L_{i,j}\right] \right) \quad (22)$$

where $d_{\min}^2\left[(x_{0,i},\ y_{0,i},\ z_{0,i}), L_{i,j}\right]$ denotes the minimum distance between plane $L_{i,j}$ and $(x_{0,i},\ y_{0,i},\ z_{0,i})$. Note that this is a general convex quadratic minimization problem since $d_{\min}[(x_{0,i},\ y_{0,i},\ z_{0,i}),\ L_{i,j}]$ is a linear function of the $(x_{0,i},\ y_{0,i},\ z_{0,i})$. To identify $d_{\min}((x_{0,i},\ y_{0,i},\ z_{0,i}),\ L_{i,j})$, we need to find the point on the plane $L_{i,j}$ closest to $(x_{0,i},\ y_{0,i},\ z_{0,i})$. For any $\mathbf{w} \in \mathbb{R}^{\mathbf{3}}$. the point $\Xi_{j,i}[\mathbf{w}]$ on the

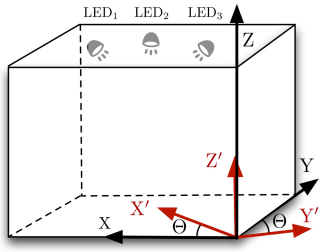

Fig. 6. Mismatch between the two coordinate systems.

plane $L_{i,j}$ that is closest to $\mathbf{w}$ is given by

$$\Xi_{j,i}[\mathbf{w}] = \mathbf{w} + E_{i,j}\mathbf{w} + F_{i,j} \tag{23}$$

where $E_{i,j}$ and $F_{i,j}$ are defined as follows:

$$E_{i,j} \triangleq \frac{-1}{a_{i,j}^2 + b_{i,j}^2 + c_{i,j}^2} \begin{bmatrix} a_{i,j} & b_{i,j} & c_{i,j} \end{bmatrix}^T \begin{bmatrix} a_{i,j} & b_{i,j} & c_{i,j} \end{bmatrix} \tag{24}$$

$$F_{i,j} \triangleq \frac{\delta_{i,j}}{a_{i,j}^2 + b_{i,j}^2 + c_{i,j}^2} \begin{bmatrix} a_{i,j} & b_{i,j} & c_{i,j} \end{bmatrix}^T. \tag{25}$$

Alternately, vector $\hat{\mathbf{V}}_i$ given in (22) can also be defined as

$$\hat{\mathbf{V}}_i = \arg\min_{\mathbf{w}} \left(\sum_{j=1}^{K} \|\Xi_{j,i}[\mathbf{w}] - \mathbf{w}\|^2 \right) \tag{26}$$

where

$$\|\Xi_{j,i}[\mathbf{w}] - \mathbf{w}\|^2 = 2F_{i,j}^T E_{i,j}\mathbf{w} + \|\mathbf{E_{i,j}w}\|^2 + \|\mathbf{F_{i,j}}\|^2. \tag{27}$$

The following result then identifies $\hat{\mathbf{V}}_i$ from (27).

Lemma 1: Let the K planes identified for the Transmitter T_i be $L_{i,j} : a_{i,j}X + b_{i,j}Y + c_{i,j}Z = \delta_{i,j}$, $j = 1, \ldots, K$. Let $\hat{\mathbf{V}}_i = [\hat{x}_{0,i}\ \hat{y}_{0,i}\ \hat{z}_{0,i}]^T$ be defined by (22). Then,

$$\hat{\mathbf{V}}_i = -\left(\sum_{j=1}^{K} E_{i,j}^T E_{i,j} \right)^{-1} \left(\sum_{j=1}^{K} E_{i,j}^T F_{i,j} \right)$$

where $E_{i,j}$ and $F_{i,j}$ are defined by (24) and (25).

Proof: This result follows directly from the solution to the quadratic optimization problem in [21, p. 458]. ■

After computing $\hat{\mathbf{V}}_i, i = 1, 2, 3$, we can estimate the position of the receiver as follows. First, note that the coordinate system of the mobile device may not match the coordinate system of the room as shown in Fig. 6. The aforementioned $\hat{\mathbf{V}}_i$'s are computed according to the mobile device's coordinate system. Before we estimate the receiver position, we must first obtain the relation between these two coordinate systems. To do so, note that we can easily align the Z-axes of both systems using gravity. We then are left with identifying the appropriate rotation in the XY plane needed to align the two coordinate systems, which is described as follows.

Definition 2: Let a coordinate system with the origin being one of the corners of the room be given. For $i = 1, 2, 3$, let $\boldsymbol{t}_i$ denote the location of transmitter T_i in this coordinate system. For $i = 1, 2, 3$, let $\boldsymbol{G}_i$ be a scaled version of $\mathbf{V}_i$ such that Z-coordinate in $\boldsymbol{G}_i$ equals the Z-coordinate of $\boldsymbol{t}_i$. For any $(i, j) \in \{(1, 2), (1, 3), (2, 3)\}$, define

$$\hat{\gamma}_{ij} \triangleq \arccos\left(\frac{(\mathbf{G}_j - \mathbf{G}_i)}{|\mathbf{G}_j - \mathbf{G}_i|} \cdot \frac{(\mathbf{t}_j - \mathbf{t}_i)}{|\mathbf{t}_j - \mathbf{t}_i|} \right). \tag{28}$$

Note that when noise is absent, $\hat{\gamma}_{12} = \hat{\gamma}_{13} = \hat{\gamma}_{23}$, since each of these is exactly the angle between the two coordinate systems. However, due to the presence of noise in the measurements, they will not exactly match. Algorithm 1 presents the steps that use above angles to estimate the receiver's position.

Algorithm 1 Three-Dimensional Positioning Algorithm

1: Let $\hat{\mathbf{V}}_i$, $i = 1, 2, 3$ be the estimated vector (from the Receiver R towards Transmitter T_i) w.r.t. the receiver's coordinate system calculated using Lemma 1.

2: Pick $(i, j) \in \{(1, 2), (1, 3), (2, 3)\}$. Do the following:

(a) Define $\hat{\mathbf{V}}_{new,i}^{(ij)}$ and $\hat{\mathbf{V}}_{new,j}^{(ij)}$ to be vectors $\hat{\mathbf{V}}_i$ and $\hat{\mathbf{V}}_j$ rotated by the angle $\hat{\gamma}_{ij}$ in (28), respectively.

(b) Let $\hat{\alpha}_{ij}$ be the angle between $\hat{\mathbf{V}}_{\text{new},i}^{(ij)}$ and $\hat{\mathbf{V}}_{\text{new},j}^{(ij)}$

$$\hat{\alpha}_{ij} \triangleq \arccos\left(\frac{\hat{\mathbf{V}}_{new,i}^{(ij)} \cdot \hat{\mathbf{V}}_{new,j}^{(ij)}}{|\hat{\mathbf{V}}_{new,i}^{(ij)}||\hat{\mathbf{V}}_{new,j}^{(ij)}|} \right). \tag{29}$$

(c) Let $\hat{\beta}_{ij}$ denote the angle between $\hat{\mathbf{V}}_{new,j}^{(ij)}$ and $\mathbf{t}_j - \mathbf{t}_i$

$$\hat{\beta}_{ij} \triangleq \arccos\left(\frac{\hat{\mathbf{V}}_{new,j}^{(ij)} \cdot (\mathbf{t}_j - \mathbf{t}_i)}{|\hat{\mathbf{V}}_{new,j}^{(ij)}||\mathbf{t}_j - \mathbf{t}_i|} \right). \tag{30}$$

(d) The estimate of the distance between Receiver R and Transmitter T_i is

$$\hat{d}_i^{(ij)} \triangleq \frac{|\mathbf{t}_j - \mathbf{t}_i| \sin\hat{\beta}_{ij}}{\sin\hat{\alpha}_{ij}},$$

and the estimated position of Receiver R using (i, j) is

$$\hat{\mathbf{S}}^{(ij)} \triangleq \mathbf{t}_i + \hat{d}_i^{(ij)} \left(\frac{-\hat{\mathbf{V}}_{\text{new},i}^{(ij)}}{|\hat{\mathbf{V}}_{\text{new},i}^{(ij)}|} \right) \tag{31}$$

3: The estimate of the Receiver R's position is defined as

$$(\hat{x}_R, \hat{y}_R, \hat{z}_R) \triangleq \tfrac{1}{3}(\hat{\mathbf{S}}^{(12)} + \hat{\mathbf{S}}^{(23)} + \hat{\mathbf{S}}^{(13)}). \tag{32}$$

VI. Results

We present our results in four parts. We first describe the experimental setup. We next present a modelling of the noise in the electric current domain that is derived from the measurements obtained from our experimental setup. We then present a section with simulation results detailing the effect of photodiode and accelerometer noise which uses the developed noise model. Finally, we present the results that are purely from our experimental setup.

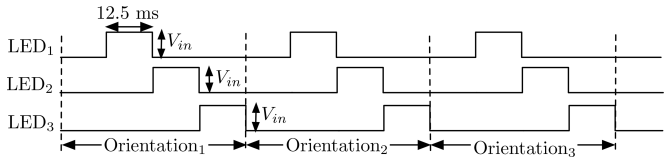

Fig. 7. TDMA scheme implemented in LabVIEW.

A. Experimental Setup

The setup consist of three Bridgelux LEDs (BXRA-56C5300-H-00) as transmitters, each of which has a typical luminous flux of $\Phi = 6000$ lumens [23]. The LEDs are located in a space of length 5 m, breadth 3 m and height 3 m at locations whose coordinates (in m) are: (3, 1.58, 3), (3.61, 2.28, 3) and (4, 1.58, 3). We assume that the receiver knows the coordinates of the transmitters whereas in practice, each transmitter can broadcast its location via VLC. A Centronic Silicon photodetector is used to measure the incident light intensity at the receiver [22]. The responsivity of this photodiode is $R_p = 22$ nA/lux, its effective area $\mathtt{A} = 15\,\text{mm}^2$, and its FoV is 1.22 rad. By measuring the light intensity at multiple incident angles, the Lambertian parameter M of the photodiode was found to be $M = 1.4$. The photodiode is operated in reverse bias mode.

In our experiments, we implement the TDMA of Fig. 7. We use LabVIEW and National Instruments Data Acquisition (DAQ) box USB-6341 to control the three LEDs. The analog port of the DAQ device is also used to measure the photodiode output. We divide time into cycles of 50 ms. Each cycle consists of four slots of equal duration. In the first slot, all LEDs are off. This slot is used to estimate the background light intensity. The remaining three slots correspond to the three transmitting LEDs. More specifically, for $1 \le i \le 3$, Transmitter T_i is on only during the $(i+1)^{\text{th}}$ slot so that the receiver can measure the received power from each transmitter separately. The receiver is assumed to know the order in which LEDs are on. The receiver identifies durations with small incident optical power as the first slot, i.e., start of a cycle. The receiver then uses the known order of LEDs to measure the incident optical power from each LED. In practical settings, the transmission order of LEDs can be communicated through visible light. It is assumed that the orientation of the receiver is kept constant during each cycle so the measurements in each slot corresponds to the same orientation. Since the cycle duration is small, the orientation can even be assumed to be constant over a few cycles.

Let for $i = 1, 2, 3$, $\Phi_{T\,i}$ denote the optical flux emitted by Transmitter T_i. For a fixed receiver orientation, let for $i = 1, \ldots, 4$, P_{Ri} (in lux $\cdot$ m^2) denote the optical power incident on the receiver in the ith slot. Then, $P_{R1} \triangleq P_{\text{Background}}$ denotes the background optical power due to other sources. Thus,

$$P_{Ri+1} = \lambda_i \Phi_{T\,i} + P_{\text{Background}}, \quad i = 1, 2, 3 \qquad (33)$$

where λ_i is the corresponding path loss term. For each slot $i = 1, 2, 3, 4$, samples of the photodiode output I_{Ri} are measured using the DAQ device. Note that by the physics of the photodiode, $\mu_{I_{R\,i}} = R_p \frac{P_{R\,i}}{\mathtt{A}}$. Hence, for $i = 1, 2, 3$, we use $(\mu_{I_{R\,i+1}} - \mu_{I_{R\,1}}) = R_p \frac{(P_{R\,i+1} - P_{\text{Background}})}{\mathtt{A}}$ as the estimate of the optical power received from Transmitter T_i. Fig. 8 illustrates a typical output from the photodiode.

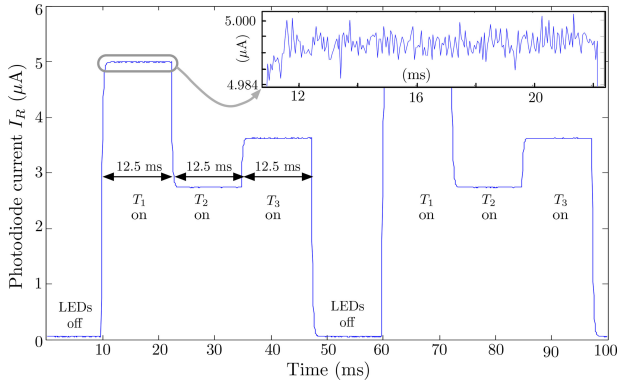

Fig. 8. A typical photodiode current measurement output.

TABLE I
VARIATION OF PHOTODIODE CURRENT'S MEAN AND VARIANCE WITH THE LED INPUT VOLTAGE AND ITS MMSE BEST-FIT FROM (35)

V_{in} (V)	μ_{I_R} (A)	$\sigma^2_{I_R}$ ((nA)^2)	Best-fit σ^2_{noise}((nA)^2)
22	1.2465×10^{-6}	40.94579	31.31379
22.5	2.1157×10^{-6}	36.75509	47.55856
23	3.2557×10^{-6}	39.90773	68.86402
23.5	3.9014×10^{-6}	75.43253	80.93125
24	4.9927×10^{-6}	99.76932	101.3279
24.5	5.7500×10^{-6}	124.3752	115.4802
25	6.7882×10^{-6}	147.1357	134.8838

B. Measurement and Modeling of Noise

The performance of our algorithm in the above experimental setup will be affected by noise in accelerometer measurements as well as noise in the electrical measurements of the photodiode, which includes shot and thermal noises. To calculate the accelerometer noise, we record the accelerometer samples by placing the receiver on a fixed surface and measuring the orientation using the device. From extensive measurements, the accelerometer noise variance was found to be $\sigma^2_W = 5.6918 \times 10^{-5}\ (\text{m/s}^2)^2$.

To measure the noise from the photodiode, we use a single LED for transmission and fix the positions of the LED and the receiver. We vary the voltage V_{in} applied to the LED in steps of 0.5 V from 22 to 25 V, which is the operating range of the LED [23]. This controls the optical flux emitted by the LED. For each V_{in}, we sample the photodiode current at a rate of 1000 samples/s for a period of 40 s. For each applied voltage, we then compute the mean μ_{I_R} and variance $\sigma^2_{I_R}$ of the photodiode electric current. Table I shows the mean and variance of the received samples for different applied voltages.

To match the noise measurements of Table I with theoretical models for shot and thermal noises, we find the minimum mean-square error (MMSE) affine fit for the measured noise

$\sigma^2_{I_R}$ (in A^2), and is given by

$$\sigma^2_{I_R} \triangleq \sigma^2_{\text{noise}} = \sigma^2_{\text{thermal}} + \sigma^2_{\text{shot}} \tag{34}$$

$$\approx 8.0185 \times 10^{-18} + 1.869 \times 10^{-11} \mu_{I_R}. \tag{35}$$

From the model, it is seen that when the average current generated by the photodiode is over 0.429 μA (equivalently, when the incident optical power is over 3×10^{-4} lux $\cdot$ m^2), the shot noise and the thermal noises contribute equally to the noise variance. In our experiments, the average current generated by a photodiode located 4 m from an LED emitting a flux of 6000 lumens when the orientation is such that $\phi = \psi = \frac{\pi}{3}$ rad is 0.498 μA. Hence, in measurements, the shot noise typically contributes more to the overall noise variance; however, the thermal noise component cannot be ignored.

C. Simulation Results

Before we present the results from our experimental setup, we present a simulation indicating how position error varies with noise in accelerometer measurements and photodiode current measurements. To do so, we simulate our algorithm in a typical room scenario where three transmitters are located at $(1, 4, 4)$, $(4, 1, 4)$ and $(4, 4, 4)$. We assume that each transmitter outputs the same luminous flux. The receiver is located at $(2, 2, 1)$. Simulation parameters are: LED half power-angle $\phi_{1/2} = \frac{\pi}{3}$ rad, receiver's Lambertian parameter $M = 1.4$, receiver's responsivity $R_p = 22$ nA/lux (see [22]) and number of orientations $K = 3$.

We also assume that a TDMA system such as that given in Section A is in place so that optical power received from different transmitters can be measured separately. We also assume that the incident power is predominantly the LoS component, and assume the mean current generated by the light from Transmitter T_i is given by $\mu_{I_{Ri}} = R_p \frac{P_{\text{LOS}i}}{\mathtt{A}}$, where $P_{\text{LOS}i}$ is computed using (2).

We assume that the photodiode is affected by both shot and thermal noises, and is given by (35). We also assume that the accelerometer measurements of acceleration due to gravity is affected by a noise with variance σ^2_W. We randomly select 3 linearly independent normal vectors $\mathbf{W_j}$, $j = A, B, C$, each representing the accelerometer measurements (in $\mathrm{m/s}^2$) for the three orientations. Each of these vectors has a magnitude equal to the acceleration due to gravity $g = 9.8$ $\mathrm{m/s}^2$. Due to various noises, the measured normal vector and photodiode-generated current $I_{Ri,j}$ (in A) for $i = 1, 2, 3$, and $j = A, B, C$, are

$$\hat{\mathbf{W}}_j = \mathbf{W}_j + (E^x_j, E^y_j, E^z_j) \tag{36}$$

$$I_{Ri,j} = \mu_{I_{Ri,j}} + E_{i,j} = R_p \frac{P_{\text{LoS}i,j}}{\mathtt{A}} + E_{i,j} \tag{37}$$

where $(E^x_j, E^y_j, E^z_j) \sim \mathcal{N}(0, \sigma^2_W \mathbb{I}_3)$ represents the accelerometer noise, and $E_{i,j} \sim \mathcal{N}(0, \sigma^2_{\text{noise,i}})$ represents the noise in the photodiode. Here, $\mathbb{I}_3$ denotes the 3×3 identity matrix. Fig. 9 presents the simulation results for position errors for different values of the luminous flux emitted by the LEDs and σ^2_W. Each point in the figure is generated by repeating the simulations 50 000 times to average out noise. Note that the three orientations

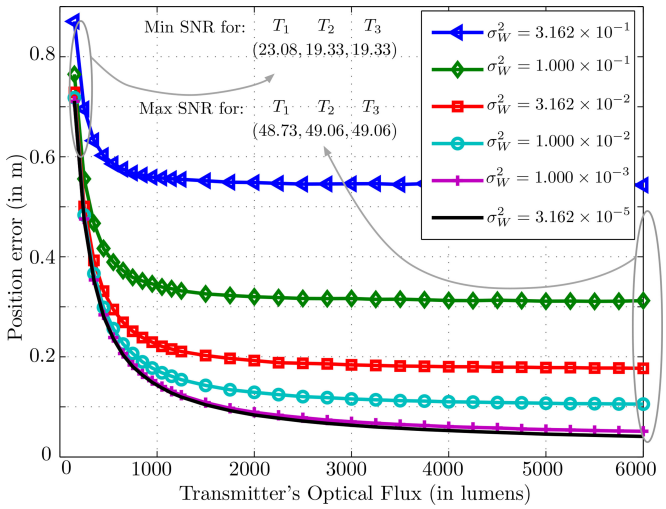

Fig. 9. Position error due to noise in accelerometer for different luminous flux. Also indicated are the highest and lowest SNRs (in dB) for each transmitter observed during simulations.

are kept constant for each of the 50 000 trials. Since the SNR varies with the LED and the orientation, only the least and the highest SNRs for each of the LEDs and for the two extremes of the transmit luminous flux are indicated in the figure. The left triple indicates the least SNRs for T_1, T_2, and T_3, respectively, and the right triple indicates the highest SNRs found during simulation.

It is noted that the position error drops rapidly with the increase in the luminous flux, and the floor is determined by the noise in accelerometer measurements. Furthermore, the figure shows that the noise in the received signal dominates the effect of noise in accelerometer measurements when the luminous flux is below 1500 lm. The effect of accelerometer noise dominates when the luminous flux is greater than 2500 lm. Note that the typical optical flux emitted by the LEDs in our experiments is between 5000–6000 lm. The figure shows that at low luminous fluxes, the position error can be around 0.8 m. Although a position error of 0.8 m is acceptable for indoor navigation, the positioning accuracy when the luminous flux is low can be improved by taking more samples of the received signal, by pointing receiver towards the LEDs, and by taking more measurements in different orientations.

D. Experimental Results

As our positioning algorithm is based on measurements at different orientations, we use the accelerometer of the smartphone to measure the orientation of the receiver. In these experiments, $K = 10$ measurements were used. In all our results, we define the position error as the distance between the estimated position and the actual position. Fig. 10 shows the benefit of using the rotation matrix in Definition 2 that aligns the coordinate system of the room with that of the receiver. The figure compares the position error with and without rotational correction. When the angle between the coordinate systems of the room and the receiver is nearly zero, it is seen that the same position error is

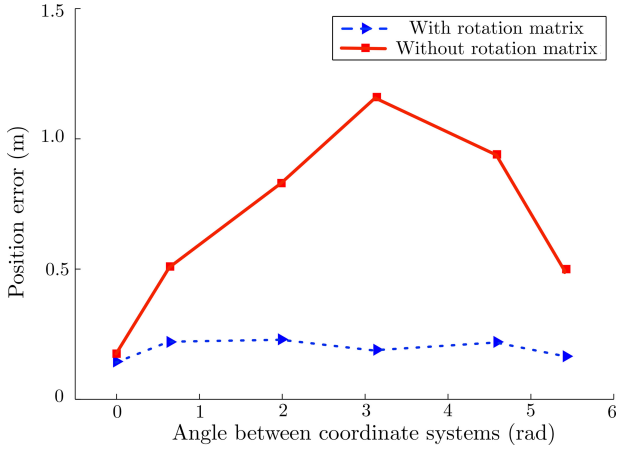

Fig. 10. Position error with and without rotational correction versus the angle between the two-coordinate systems.

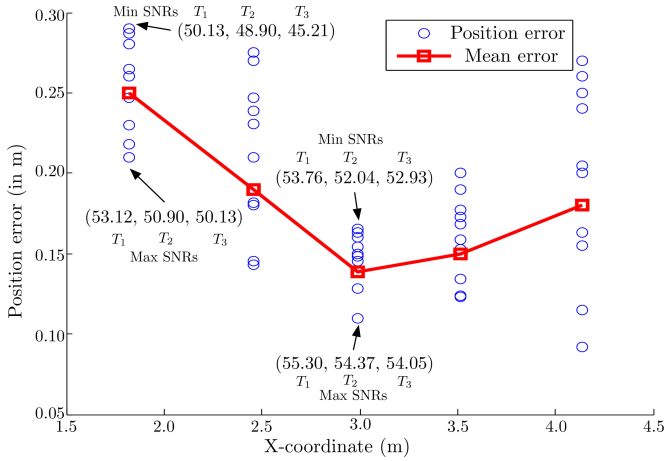

Fig. 11. Position error at location (x, 1.8, 0.71). Here, the receiver was not pointed towards the LEDs for all orientations. This allows us to observe the effect of non-LoS paths.

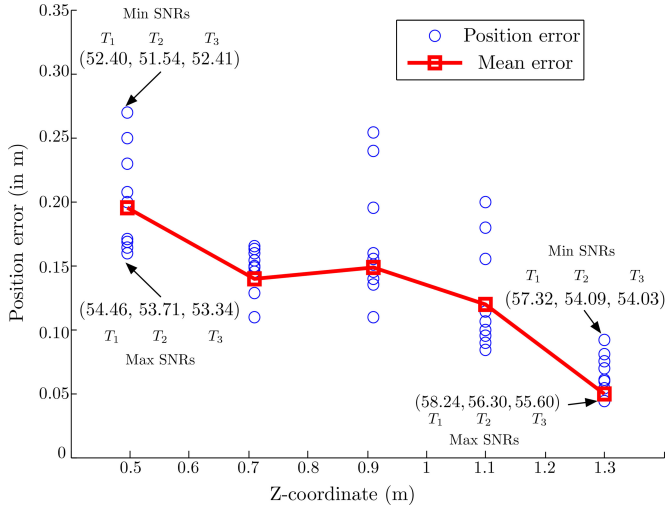

Fig. 12. Position error at location (2.99, 1.79, z). Here, the receiver was not pointed towards the LEDs for all orientations. This allows us to observe the effect of non-LoS paths.

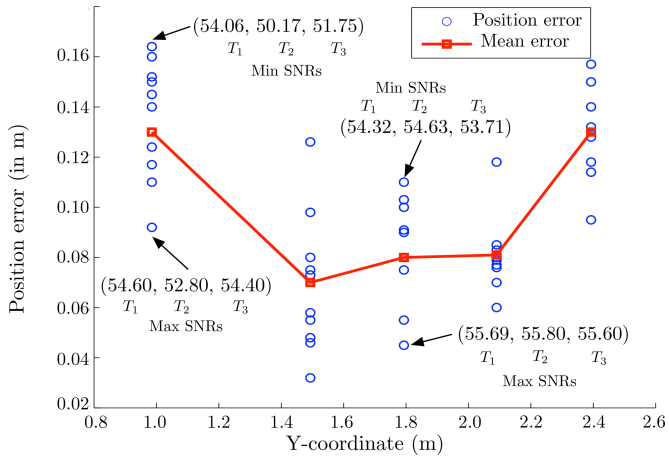

Fig. 13. Position error at location (3.5, y, 0.71).

observed with or without rotation. However, if the coordinate systems of the room and the receiver are different, the position error is significantly larger without the use of the proper rotation matrix. The maximum error occurs when the angle between the coordinate systems is π rad.

We now present the experimental results for position error as a function of the location of the receiver. These results are presented in Figs. 11–13, and in each figure, we fix two coordinates of the receiver and vary only the third. At each position, we perform the experiment 10 times, each time with a different receiver orientation. The orientations of the receiver are chosen randomly such that the incidence angles (in radians) lie in $(0, \frac{\pi}{3})$. These results show the error distributions and the mean position errors for different positions in the room. To gauge the SNRs in these experiments, the noise power model of (35), which is also derived from experiments is used. As the SNR depends on the orientation, the receiver location, and the transmitter, these figures also indicate the highest and lowest SNR recorded for each LED at the location with the highest and the lowest mean position error. For example, in Fig. 11, the location (1.8, 1.8, 0.71) corresponds to the highest mean position error. In this location, among the orientations for which measurements were taken, the lowest SNRs (in dB) for the signals from LED_1, LED_2 and LED_3 are (50.13, 48.90, 45.21), respectively, and the highest recorded SNRs (in dB) are (53.12, 50.90, 50.13), respectively.

The typical SNR range calculated using three LEDs and photodiode in a space of length 5 m, breadth 3 m and height 3 m is 45 to 58.5 dB, where 58.5 dB is achieved when the receiver is in the centre of the room at a height of 1.3 m.

In Figs. 11 and 12, the position errors at various locations are shown. In these measurements, few receiver orientations are chosen pointing away from the transmitters (e.g., towards the wall of the room, which is 1.8 m away from the receiver).The results in Fig. 11 are obtained when the receiver is varied along the X-axis but the Y- and Z-coordinates are kept fixed at 1.8 m and 0.71 m, respectively. The mean position error is lower than

0.15 m when the receiver is in the center of the room. This is due to the high SNRs of the signals from the three LEDs, because the distance from each the transmitters is smaller here than when the receiver is in a corner of the room. The mean position error increases to 0.25 m when the receiver is away from the center.

The results in Fig. 12 are obtained when the receiver is varied along the *Z*-axis. The *X*- and *Y*-coordinates are fixed at 2.99 and 1.79 m, respectively. It is noted that for the receiver's height of 1.3 m, which is the nominal receiver's height if the user is standing and holding the mobile device in hand, the maximum position error is less than 0.1 m and the mean position error is 0.055 m.

The results in Fig. 13 are obtained when the position of the receiver is varied along *Y*-axis. The *X*-coordinate and *Z*-coordinate of the receiver are fixed at 3.5 and 0.71 m, respectively. In these measurements, the receiver is pointed towards the transmitters.

This results in higher received power form the LoS path, and consequently, better accuracy of the position estimate. For example, the point (3.5, 1.8, 0.71) appears in both Figs. 11 and 13, but with different mean errors. This is because the effect of received optical power from non-LoS paths in measurements/orientations chosen for Fig. 13 are lesser than than the measurements chosen for Fig. 11, and hence, the positioning accuracy is better.

From the experiments, we can see that the received power from non-LoS paths is not negligible, especially when the receiver is facing towards the wall of the room or if there are reflective objects in the FoV of the receiver. Hence, positioning accuracy is also affected by the received power from non-LoS paths. This effect on positioning accuracy can be visualized by comparing Figs. 11 and 13. Since our algorithm depends on the ratio of received LoS powers at different orientations, it is possible that in one observation the LoS term is dominant, and in the other, the non-LoS is dominant. By taking the ratio, we will be comparing P_{LoS} of one measurement with the P_{NLoS} of another, instead of comparing the LoS terms. Hence, multi-path signal can affect adversely the ratio of received powers, and consequently, decreases the positioning accuracy. Incorporating multi-path effects requires a more complicated optical channel model, which is beyond the scope of this work. It is nevertheless encouraging to note that when the average distances between the receiver and transmitters are small and the receiver is pointed towards LEDs, positioning accuracy of within a few centimeters is attainable. In fact, when the receiver is pointed towards the LEDs, the average position error along the breadth of the room is less than 0.14 m.

VII. Conclusion

We have proposed an indoor positioning system that uses VLC and accelerometer measurements. The proposed system uses received light intensity and accelerometer measurements to compute distances between the transmitters and the receiver. Accelerometer measurements are used to eliminate the need for commonly-used assumptions in the literature. Our algorithm does not require costly equipment, and has low complexity. Extensive experimentations in an office environment and simulations have been done to evaluate the performance of our algorithm. Our system offers good positioning accuracy even for receivers with wider field of view (FoV). Experimental results show that an average position error of less than 0.25 m is achievable. An important observation from the experimental results is that the positioning accuracy depends not only on the distances between transmitters and receiver, but also on the orientation of the receiver. Lastly, position errors within a few centimeters is achievable, provided the receiver is under three LEDs and pointing towards them.

References

[1] C. Drane, M. Macnaughtan, and C. Scott, "Positioning GSM telephones," *IEEE Commun. Mag.*, vol. 36, no. 4, pp. 46–54, Apr. 1998.

[2] M. Vossiek, L. Wiebking, P. Gulden, J. Wieghardt, C. Hoffmann, and P. Heide, "Wireless local positioning," *IEEE Microw. Mag.*, vol. 4, no. 4, pp. 77–86, Dec. 2003.

[3] J. Hightower and G. Borriello, "Location systems for ubiquitous computing," *Computer*, vol. 34, no. 8, pp. 57–66, Aug. 2001.

[4] A. Yazici, U. Yayan, and H. Yucel, "An ultrasonic based indoor positioning system," in *Proc. Int. Symp. Innov. Intell. Syst. Appl.*, Jun. 2011 pp. 585–589.

[5] N. Arrue, M. Losada, L. Zamora-Cadenas, A. Jiménez-Irastorza, and I. Vélez, "Design of an IR-UWB Indoor localization system based on a novel RTT ranging estimator," in *Proc. 1st Int. Conf. Sens. Device Technol. Appl.*, Jul. 2010 pp. 52–57.

[6] P. Bahl and V. Padmanabhan, "RADAR: An in-building RF-based user location and tracking system," in *Proc. 19th Annu. Joint Conf. IEEE Comput. Commun. Soc.*, Mar. 2000, vol. 2, pp. 775–784.

[7] Y. Gu, A. Lo, and I. Niemegeers, "A survey of indoor positioning systems for wireless personal networks," *IEEE Commun. Surveys Tuts.*, vol. 11, no. 1, pp. 13–32, First Quarter 2009.

[8] H. Liu, H. Darabi, P. Banerjee, and J. Liu, "Survey of wireless indoor positioning techniques and systems," *IEEE Trans. Syst., Man, Cybern. C, Appl. Rev.*, vol. 37, no. 6, pp. 1067–1080, Nov. 2007.

[9] W. Zhang and M. Kavehrad, "A 2-D indoor localization system based on visible light LED," in *Proc. IEEE Photon. Soc. Summer Top. Meet. Series*, Jul. 2012 pp. 80–81.

[10] G. Cossu, M. Presi, R. Corsini, P. Choudhury, A. Khalid, and E. Ciaramella, "A visible light localization aided optical wireless system," in *Proc. IEEE GLOBECOM Workshop*, Pisa, Italy, Dec. 2011, pp. 802–807.

[11] H. Kim, D. Kim, S. Yang, Y. Son, and S. Han, "An indoor visible light communication positioning system using a RF carrier allocation technique," *J. Lightw. Technol.*, vol. 31, no. 1, pp. 134–144, Jan. 2013.

[12] C. Sertthin, T. Ohtsuki, and M. Nakagawa, "6-axis sensor assisted low complexity high accuracy-visible light communication based indoor positioning system," *IEICE Trans. Commun.*, vol. E93-B, no. 11, pp. 2879–2891, Nov. 2010.

[13] S.-H. Yang, E.-M. Jeong, and S.-K. Han, "Indoor positioning based on received optical power difference by angle of arrival," *IEEE Electron. Lett.*, vol. 50, no. 1, pp. 49–51, Jan. 2014.

[14] A. Arafa, X. Jin, and R. Klukas, "Wireless indoor optical positioning with a differential photosensor," *IEEE Photon. Technol. Lett.*, vol. 24, no. 12, pp. 1027–1029, Jun. 2012.

[15] S.-Y. Jung, S. Hann, and C.-S. Park, "TDOA-based optical wireless indoor localization using LED ceiling lamps," *IEEE Trans. Consum. Electron.*, vol. 57, no. 4, pp. 1592–1597, Nov. 2011.

[16] F. Gfeller and U. Bapst, "Wireless in-house data communication via diffuse infrared radiation," *Proc. IEEE*, vol. 67, no. 11, pp. 1474–1486, Nov. 1979.

[17] T. Komine and M. Nakagawa, "Fundamental analysis for visible-light communication system using LED lights," *IEEE Trans. Consum. Electron.*, vol. 50, no. 1, pp. 100–107, Feb. 2004.

[18] J. Kahn and J. Barry, "Wireless infrared communications," *Proc. IEEE*, vol. 85, no. 2, pp. 265–298, Feb. 1997.

[19] M. Kjaergaard and C. Munk, "Hyperbolic location fingerprinting: A calibration-free solution for handling differences in signal strength," in *Proc. 6th Annu. IEEE Int. Conf. Pervasive Comput. Commun.*, Mar. 2008, pp. 110–116.

[20] P. Krishnan, A. S. Krishnakumar, W.-H. Ju, C. Mallows, and S. Gamt, "A system for LEASE: Location estimation assisted by stationary emitters for indoor RF wireless networks," in *Proc. 23rd Annu. Joint Conf. IEEE Comput. Commun. Societies*, Mar. 2004, pp. 1001–1011.
[21] S. Boyd and L. Vanderberghe, *Convex Optimization*. Cambridge, U.K.: Cambridge Univ. Press, 2012.
[22] Centronic Eye Response Detector Series-E Photodiode (OSD15-E). (2014). [Online]. Available: http://www.centronic.co.uk/downloads.htm
[23] Bridgelux RS Array Series LED. (2011). [Online]. Available: http://www.leds.de/out/media/Bridgelux.pdf

Muhammad Yasir (S'13) received the B.Eng. degree in electrical engineering from Air University, Islamabad, Pakistan, in 2008. He received the M.S. degree in communications system engineering from the National University of Science and Technology, Islamabad, in 2011. Since 2012, he has been with the Institute for Telecommunications Research, University of South Australia, where he is currently working toward the Ph.D. degree. His research interests include visible light communications and positioning systems.

Siu-Wai Ho (S'05–M'07) received the B.Eng., M.Phil., and Ph.D. degrees in information engineering from the Chinese University of Hong Kong, Hong Kong, in 2000, 2003, and 2006, respectively. During 2006 to 2008, he was a Postdoctoral Research Fellow with the Department of Electrical Engineering, Princeton University, Princeton, NJ, USA. Since 2009, he has been with the Institute for Telecommunications Research, University of South Australia, Adelaide, S.A., Australia, where he is currently a Senior Research Fellow. His current research interests include Shannon theory, visible light communications, information-theoretic security, and biometric security systems. Dr. Ho received the Croucher Foundation Fellowship for 2006–2008, the 2008 Young Scientist Award from the Hong Kong Institution of Science, UniSA Research SA Fellowship for 2010–2013, and the Australian Research Council Australian Postdoctoral Fellowship for 2010–2013.

Badri N. Vellambi (M'09) received the B.Tech. degree in electrical engineering) from the Indian Institute of Technology Madras, Chennai, India, in 2002, and the M.S. degree in electrical engineering, the M.S. degree in mathematics, and the Ph.D. degree in electrical engineering from the Georgia Institute of Technology, Atlanta, GA, USA, in 2005, 2008, and 2008, respectively. Since 2008, he has been a Research Fellow with the Institute for Telecommunications Research, University of South Australia, Adelaide, S.A., Australia. His current research interests include Shannon theory, channel coding, multiuser information theory, and communications theory.